

Derivation of the Cross-Free Family representation for the box diagram

Zeno Capatti^a

^a*Institute for Theoretical Physics, University of Bern,
Sidlerstrasse 5, 3012, Bern
Switzerland*

E-mail: zeno.ca@gmail.com

I work out in full detail the derivation of the Cross-Free Family (CFF) representation for the box diagram, and highlight the differences with its Time Ordered Perturbation Theory (TOPT) representation. I briefly discuss implications for the threshold singularity structure of the diagram.

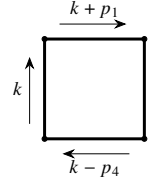
*RADCOR 2023 – 16th International Symposium on Radiative Corrections: Applications of Quantum Field Theory to Phenomenology,
Sunday 28th May 2023 - Friday 2nd June 2023,
Crieff, Scotland.*

1. Introduction

This document contains an explicit example of the derivation of the Cross-Free Family representation hypothesized in ref. [1] and then derived systematically in ref. [2]. It is a three-dimensional representation [2–16] in which the threshold singularity structure of the Feynman diagram becomes especially constrained and in which spurious singularities are absent. These constraints are related to the graph-theoretic notions of connectedness and crossing that recur often in analyses of the singularity structure of Feynman diagrams [16–25], and will be derived by using tools from graph-theory and convex geometry (specifically, by using properties of Fourier transforms of polytopes [26]). In [27], a novel and interesting derivation of the representation based on posets has been proposed. We are interested in performing analytically the following integral

$$f_{\square}^{3d} = \int \frac{dk^0}{2\pi} \frac{\mathcal{N}(\{k^0 + p_{1i}^0\}_{i=1}^4; \{\vec{k} + \vec{p}_{1i}\}_{i=1}^4)}{((k + p_{11})^2 - m_1^2)((k + p_{12})^2 - m_2^2)((k + p_{13})^2 - m_3^2)((k + p_{14})^2 - m_4^2)}, \quad (1)$$

with $p_{1i} = \sum_{j=1} p_j$. The full Feynman diagram for the box diagram is written in terms of f_{\square}^{3d} as follows:



$$= \int \frac{d^3\vec{k}}{(2\pi)^3} f_{\square}^{3d}. \quad (2)$$

The Feynman diagram corresponds to a graph which is characterised by a set of vertices, $\mathcal{V} = \{v_1, v_2, v_3, v_4\}$, and edges, $\mathcal{E} = \{e_1, e_2, e_3, e_4\}$, with labels assigned according to the following convention



$$. \quad (3)$$

We are ready to start deriving the Cross-Free Family representation.

2. Acyclic graphs

We introduce one auxiliary integration variable for each edge, named q_i^0 , which simply equals the energy flowing through that edge, expressed as a linear combination of the energy loop variable k^0 and the energies of the external momenta

$$f_{\square}^{3d} = \int \frac{dk^0}{2\pi} \int \left[\prod_{i=1}^4 \frac{dq_i^0}{(q_i^0)^2 - E_i^2} \delta(q_i^0 - k^0 - p_{1i}^0) \right] \mathcal{N}(\{q_i^0\}_{i=1}^4; \{\vec{k} + \vec{p}_{1i}\}_{i=1}^4), \quad (4)$$

having introduced the on-shell energies

$$E_i = \sqrt{|\vec{k} + \vec{p}_{1i}|^2 + m_i^2 - i\varepsilon}. \quad (5)$$

We also suppressed the dependence on the spatial components of the momenta in the numerator, for the sake of compactness. Using the Fourier representation of the Dirac delta function, we obtain

$$f_{\square}^{3d} = \int \frac{dk^0}{2\pi} \int \left[\prod_{i=1}^4 \frac{dq_i^0 d\tau_i}{2\pi} \frac{\exp\{i\tau_i (q_i^0 - k^0 - p_{1i}^0)\}}{(q_i^0)^2 - E_i^2} \right] \mathcal{N}(\{q_i^0\}_{i=1}^4),$$

which can be re-written in order to highlight the simplicity of the q_i^0 integration

$$f_{\square}^{3d} = \int \frac{dk^0}{2\pi} \int \left[\prod_{i=1}^4 d\tau_i e^{i\tau_i (-k^0 - p_{1i}^0)} \right] \int \left[\prod_{j=1}^4 \frac{dq_j^0}{2\pi} \frac{e^{iq_j^0 \tau_j}}{(q_j^0)^2 - E_j^2} \right] \mathcal{N}(\{q_i^0\}_{i=1}^4). \quad (6)$$

In particular, the advantage of introducing the auxiliary integration variables is now evident: energy conservation is resolved through the oscillatory behaviour of the complex exponentials and the integration over the energies q_i^0 of each propagator is trivial to perform. In particular, the following identity holds:

$$\int \left[\prod_{j=1}^4 \frac{dq_j^0}{2\pi} \frac{e^{iq_j^0 \tau_j}}{(q_j^0)^2 - E_j^2} \right] \mathcal{N}(\{q_i^0\}_{i=1}^4) = \sum_{\vec{\sigma} \in \{\pm\}^4} \mathcal{N}(\{\sigma_i E_i\}_{i=1}^4) \prod_{j=1}^4 \frac{\Theta(-\sigma_j \tau_j) e^{i\sigma_j E_j \tau_j}}{2iE_j}, \quad (7)$$

obtained by straight-forward contour integration. Notably, such an identity holds only if the residue at infinity of the integrand, in each of the q_j^0 variables, vanishes. This in turn imposes a constraint on the shape of the numerator, namely that it can be linear at most in each of the q_i^0 variables. In other words, it must take the form

$$\mathcal{N}(\{q_i^0\}_{i=1}^4) = \sum_{i_1=0}^1 \sum_{i_2=0}^1 \sum_{i_3=0}^1 \sum_{i_4=0}^1 a_{i_1 i_2 i_3 i_4} (q_1^0)^{i_1} (q_2^0)^{i_2} (q_3^0)^{i_3} (q_4^0)^{i_4}. \quad (8)$$

Substituting eq. (7) in eq. (6), and performing the change of variables $\tau_j \rightarrow \sigma_j \tau_j$, we obtain

$$f_{\square}^{3d} = \sum_{\vec{\sigma} \in \{\pm\}^4} \frac{\mathcal{N}(\{\sigma_n E_n\}_{n=1}^4)}{\prod_{m=1}^4 2iE_m} \int \frac{dk^0}{2\pi} \int \left[\prod_{i=1}^4 d\tau_i \Theta(\tau_i) e^{-iE_i \tau_i} \right] \left[\prod_{j=1}^4 e^{-i\sigma_j \tau_j (k^0 + p_{1j}^0)} \right], \quad (9)$$

having used that $\sigma_j^2 = 1$. Finally, integration in k^0 is trivial by using the Fourier representation of the Dirac delta to rewrite the integration in k^0 . In particular

$$f_{\square}^{3d} = \sum_{\vec{\sigma} \in \{\pm\}^4} \frac{\mathcal{N}(\{\sigma_n E_n\}_{n=1}^4)}{\prod_{m=1}^4 2iE_m} \hat{\mathbf{1}}_{\vec{\sigma}}, \quad \hat{\mathbf{1}}_{\vec{\sigma}} = \int \left[\prod_{i=1}^4 d\tau_i \Theta(\tau_i) e^{-i(E_i - \sigma_i p_{1i}^0) \tau_i} \right] \delta \left(\sum_{j=1}^4 \sigma_j \tau_j \right). \quad (10)$$

The sum over vector signs $\vec{\sigma}$ can be interpreted as a sum over orientations of the edges of the box diagram. The sign vector $\vec{\sigma} = (1, 1, 1, 1)$, which we represent by assigning an arrow to the edge, corresponds to the orientation of the edges chosen for the original routing of eq. (2):

$$G_{\vec{\sigma}_1} = \begin{array}{c} \begin{array}{|c|} \hline \rightarrow \\ \hline \end{array} \\ \begin{array}{|c|} \hline \rightarrow \\ \hline \end{array} \\ \begin{array}{|c|} \hline \leftarrow \\ \hline \end{array} \\ \begin{array}{|c|} \hline \leftarrow \\ \hline \end{array} \\ \hline \end{array} \quad (11)$$

The sign vector $\vec{\sigma}_2 = (-1, -1, -1, -1)$ corresponds to the orientation obtained from that of eq. (11) by flipping the arrows of all edges. The sign vector $\vec{\sigma}_3 = (-1, 1, -1, 1)$, instead, corresponds to the orientation obtained from that of eq. (11) by flipping the arrow for the edges with momentum q_1 and q_3 :

$$G_{\vec{\sigma}_3} = \begin{array}{c} \begin{array}{|c|} \hline \rightarrow \\ \hline \end{array} \\ \begin{array}{|c|} \hline \leftarrow \\ \hline \end{array} \end{array} \quad (12)$$

In general, we can associate to $\vec{\sigma}$ the directed graph $G_{\vec{\sigma}}$ constructed in the way represented above. To conclude this section, we will now look more closely at the sum over vectors $\vec{\sigma}$ and show that two terms of this sum vanish identically. They correspond to the two vectors $\sigma_1 = (1, 1, 1, 1)$ and $\sigma_2 = (-1, -1, -1, -1)$. Indeed,

$$\hat{\mathbb{1}}_{\vec{\sigma}_1} = \int \left[\prod_{i=1}^4 d\tau_i \Theta(\tau_i) e^{-i(E_i - p_{1i}^0)\tau_i} \right] \delta(\tau_1 + \tau_2 + \tau_3 + \tau_4) = 0 \quad (13)$$

since the constraints imposed by the Heaviside theta functions, namely that $\tau_i > 0$, cannot be satisfied simultaneously with the linear constraint, imposed by the Dirac delta function, that $\tau_1 + \tau_2 + \tau_3 + \tau_4 = 0$. Looking at the directed graphs $G_{\vec{\sigma}_1}$ and $G_{\vec{\sigma}_2}$, we realise that they are all and only the directed graphs that have a directed cycle within them. In other words, we can walk starting from one of their vertices and, following the direction of the arrows, return to the original vertex. The graphs that escape this analysis are precisely those that do not have a directed cycle within them; in technical jargon, they are called *acyclic graphs*. In turn, we can write

$$f_{\square}^{3d} = \sum_{\substack{\vec{\sigma} \text{ s.t.} \\ G_{\vec{\sigma}} \text{ is acyclic}}} \frac{\mathcal{N}(\sigma_1 E_1, \sigma_2 E_2, \sigma_3 E_3, \sigma_4 E_4)}{\prod_{j=1}^4 2iE_j} \hat{\mathbb{1}}_{\vec{\sigma}}. \quad (14)$$

This result is dual to that obtained within Flow-Oriented Perturbation Theory [7]. We now briefly expand on the mathematical interpretation of the object $\hat{\mathbb{1}}_{\vec{\sigma}}$.

3. Fourier transform of cones

The Heaviside Theta functions and the Dirac delta distribution can be absorbed in a redefinition of the integration domain. More specifically, we collect the relevant integration variables in a vector $\boldsymbol{\tau} = (\tau_1, \tau_2, \tau_3, \tau_4)$, the corresponding on-shell energies in another $\mathbf{E} = (E_1, E_2, E_3, E_4)$, and finally the energy shifts of the edges in yet another vector $\mathbf{p}_{\vec{\sigma}}^0 = (\sigma_1 p_{11}^0, \sigma_2 p_{12}^0, \sigma_3 p_{13}^0, \sigma_4 p_{14}^0)$. We then define the integration domain

$$\mathcal{K}_{\vec{\sigma}} = \left\{ \boldsymbol{\tau} \in \mathbb{R}_+^4 \mid \sigma_1 \tau_1 + \sigma_2 \tau_2 + \sigma_3 \tau_3 + \sigma_4 \tau_4 = 0 \right\}. \quad (15)$$

$\mathcal{K}_{\vec{\sigma}}$ is a convex cone, as it is the intersection of the positive orthant (a convex cone) with a hyperplane. In terms of the newly-defined vectors and the cone $\mathcal{K}_{\vec{\sigma}}$, we may rewrite

$$\hat{\mathbb{1}}_{\vec{\sigma}} = \int_{\mathcal{K}_{\vec{\sigma}}} d\boldsymbol{\tau} e^{-i\boldsymbol{\tau} \cdot (\mathbf{E} - \mathbf{p}_{\vec{\sigma}}^0)} = \int_{\mathbb{R}^4} d\boldsymbol{\tau} e^{-i\boldsymbol{\tau} \cdot (\mathbf{E} - \mathbf{p}_{\vec{\sigma}}^0)} \mathbb{1}_{\vec{\sigma}}(\boldsymbol{\tau}), \quad (16)$$

i.e. the Fourier transform of the characteristic function $\mathbb{1}_{\vec{\sigma}}$ of the set $\mathcal{K}_{\vec{\sigma}}$, defined as usual:

$$\mathbb{1}_{\mathcal{K}_{\vec{\sigma}}}(\boldsymbol{\tau}) = \begin{cases} 1 & \text{if } \boldsymbol{\tau} \in \mathcal{K}_{\vec{\sigma}} \\ 0 & \text{otherwise} \end{cases}. \quad (17)$$

Following the results of the previous section, we conclude that $\mathcal{K}_{\vec{\sigma}}$ is the empty set if $G_{\vec{\sigma}}$ is not an acyclic graph. Computing the Fourier transform $\hat{\mathbb{1}}_{\vec{\sigma}}$ requires to find a triangulation of the cone $\mathcal{K}_{\vec{\sigma}}$.

4. Triangulations and the edge-contraction operation

4.1 An example

For the purposes of this section, let us focus on the directed graph corresponding to $\vec{\sigma}_3 = (-1, 1, -1, 1)$, graphically represented in eq. (12). We have, identifying $\hat{\mathbb{1}}_{\vec{\sigma}_3}$ with the graph $G_{\vec{\sigma}_3}$:

$$\begin{array}{c} v_1 \xrightarrow{e_2} v_2 \\ e_1 \downarrow \quad \uparrow e_3 \\ v_4 \xleftarrow{e_4} v_3 \end{array} = \hat{\mathbb{1}}_{\vec{\sigma}_3} = \int \left[\prod_{j=1}^4 d\tau_j \Theta(\tau_j) e^{i\tilde{E}_j \tau_j} \right] \delta(-\tau_1 + \tau_2 - \tau_3 + \tau_4), \quad (18)$$

having redefined $\tilde{E}_j = E_j - (\vec{\sigma}_3)_j p_j^0$. We now relate the process of performing time integrations with the edge-contraction operation. We start by writing

$$\Theta(\tau_1)\Theta(\tau_2) = \Theta(\tau_1 - \tau_2)\Theta(\tau_2) + \Theta(\tau_2 - \tau_1)\Theta(\tau_1), \quad (19)$$

corresponding to a triangulation of the positive orthant $\tau_1, \tau_2 > 0$ in two cones: $\tau_2 > 0, \tau_1 > \tau_2$ and $\tau_1 > 0, \tau_2 > \tau_1$. Substituted in $\hat{\mathbb{1}}_{\vec{\sigma}_3}$, we obtain

$$\begin{array}{c} v_1 \xrightarrow{e_2} v_2 \\ e_1 \downarrow \quad \uparrow e_3 \\ v_4 \xleftarrow{e_4} v_3 \end{array} = \int \left[\prod_{i=3}^4 d\tau_i \Theta(\tau_i) e^{i\tilde{E}_i \tau_i} \right] \left[\int d\tau_1 d\tau_2 e^{i\tau_1 \tilde{E}_1 + i\tau_2 \tilde{E}_2} \Theta(\tau_1)\Theta(\tau_2 - \tau_1) \delta(-\tau_1 + \tau_2 - \tau_3 + \tau_4) \right. \\ \left. + \int d\tau_1 d\tau_2 e^{i\tau_1 \tilde{E}_1 + i\tau_2 \tilde{E}_2} \Theta(\tau_2)\Theta(\tau_1 - \tau_2) \delta(-\tau_1 + \tau_2 - \tau_3 + \tau_4) \right] \quad (20)$$

We now change variables $\tau'_2 = \tau_2 - \tau_1$, $\tau'_j = \tau_j$, $j = 1, 3, 4$ for the first integral and $\tau'_1 = \tau_1 - \tau_2$, $\tau'_j = \tau_j$, $j = 2, 3, 4$ for the second one

$$\begin{array}{c} v_1 \xrightarrow{e_2} v_2 \\ e_1 \downarrow \quad \uparrow e_3 \\ v_4 \xleftarrow{e_4} v_3 \end{array} = \int \left[\prod_{i \in \{2,3,4\}} d\tau_i \Theta(\tau_i) e^{i\tilde{E}_i \tau_i} \right] \delta(\tau_2 - \tau_3 + \tau_4) \int d\tau_1 \Theta(\tau_1) e^{i\tau_1 (\tilde{E}_1 + \tilde{E}_2)} \\ + \int \left[\prod_{i \in \{1,3,4\}} d\tau_i \Theta(\tau_i) e^{i\tilde{E}_i \tau_i} \right] \delta(-\tau_1 - \tau_3 + \tau_4) \int d\tau_2 \Theta(\tau_2) e^{i\tau_2 (\tilde{E}_1 + \tilde{E}_2)}. \quad (21)$$

The nested integrations are now trivial to perform

$$\begin{aligned}
 \begin{array}{c} v_1 \xrightarrow{e_2} v_2 \\ \uparrow e_1 \quad \downarrow e_3 \\ v_4 \xleftarrow{e_4} v_3 \end{array} &= \frac{i}{\tilde{E}_1 + \tilde{E}_2} \left[\int \left[\prod_{i \in \{2,3,4\}} d\tau_i \Theta(\tau_i) e^{i\tilde{E}_i \tau_i} \right] \delta(\tau_2 - \tau_3 + \tau_4) \right. \\
 &\quad \left. + \int \left[\prod_{i \in \{1,3,4\}} d\tau_i \Theta(\tau_i) e^{i\tilde{E}_i \tau_i} \right] \delta(-\tau_1 - \tau_3 + \tau_4) \right]. \quad (22)
 \end{aligned}$$

Such an equation has a straight-forward diagrammatic representation. In particular, we recognise that it can be written as

$$\begin{array}{c} v_1 \xrightarrow{e_2} v_2 \\ \uparrow e_1 \quad \downarrow e_3 \\ v_4 \xleftarrow{e_4} v_3 \end{array} = \frac{i}{(\tilde{E}_1 + \tilde{E}_2)} \left[\begin{array}{c} v_{12} \\ e_1 \swarrow \quad \searrow e_3 \\ v_4 \quad v_3 \end{array} + \begin{array}{c} v_2 \\ e_2 \swarrow \quad \searrow e_3 \\ v_{14} \quad v_3 \end{array} \right]. \quad (23)$$

We thus recognise that the overall effect of having performed the integration in the way we have laid down is, at the graph level, equivalent to contracting one-by-one the two edges e_1 and e_2 adjacent to the vertex v_1 . It turns out that the operation can be iterated. We can now choose one vertex for each of the two contracted graphs: for the first, we choose the vertex v_4 common to e_1 and e_4 ; for the second, we choose the vertex v_2 common to e_2 and e_3 . Performing the contraction, we obtain:

$$\begin{array}{c} v_1 \xrightarrow{e_2} v_2 \\ \uparrow e_1 \quad \downarrow e_3 \\ v_4 \xleftarrow{e_4} v_3 \end{array} = \frac{i}{(\tilde{E}_1 + \tilde{E}_2)} \left[\frac{i}{(\tilde{E}_1 + \tilde{E}_4)} \left[\begin{array}{c} v_{124} \\ e_3 \swarrow \quad \searrow e_4 \\ v_3 \end{array} + \begin{array}{c} v_{12} \\ e_1 \swarrow \quad \searrow e_3 \\ v_{34} \end{array} \right] \right. \quad (24)$$

$$\left. + \frac{i}{(\tilde{E}_2 + \tilde{E}_3)} \left[\begin{array}{c} v_{124} \\ e_3 \swarrow \quad \searrow e_4 \\ v_3 \end{array} + \begin{array}{c} v_{14} \\ e_2 \swarrow \quad \searrow e_4 \\ v_{23} \end{array} \right] \right]. \quad (25)$$

We now notice that

$$\begin{array}{c} \swarrow e_1 \\ \searrow e_3 \end{array} = \begin{array}{c} \swarrow e_2 \\ \searrow e_4 \end{array} = 0, \quad (26)$$

since they are oriented in such a way to allow for a directed cycle. In other words, since these two graphs are not acyclic, the corresponding integrals vanish, because the domain of integration is empty. This implies that

$$\begin{array}{c} v_1 \xrightarrow{e_2} v_2 \\ \uparrow e_1 \quad \downarrow e_3 \\ v_4 \xleftarrow{e_4} v_3 \end{array} = \frac{i}{(\tilde{E}_1 + \tilde{E}_2)} \left[\frac{i}{(\tilde{E}_1 + \tilde{E}_4)} \begin{array}{c} v_{124} \\ e_3 \swarrow \quad \searrow e_4 \\ v_3 \end{array} + \frac{i}{(\tilde{E}_2 + \tilde{E}_3)} \begin{array}{c} v_{124} \\ e_3 \swarrow \quad \searrow e_4 \\ v_3 \end{array} \right]. \quad (27)$$

Finally, we compute the two bubble integrals explicitly. We have

$$\begin{array}{c} v_{124} \\ e_3 \swarrow \quad \searrow e_4 \\ v_3 \end{array} = \int d\tau_3 d\tau_4 \Theta(\tau_3) \Theta(\tau_4) \delta(\tau_3 - \tau_4) e^{i\tau_3 \tilde{E}_3 + i\tau_4 \tilde{E}_4} = \frac{i}{\tilde{E}_3 + \tilde{E}_4}. \quad (28)$$

Finally, we can write:

$$\begin{array}{c} v_1 \\ \begin{array}{c} \xrightarrow{e_2} v_2 \\ \leftarrow e_1 \\ \leftarrow e_3 \\ \leftarrow e_4 \\ v_4 \end{array} \end{array} = \frac{i}{(\tilde{E}_1 + \tilde{E}_2)} \left[\frac{i^2}{(\tilde{E}_1 + \tilde{E}_4)(\tilde{E}_3 + \tilde{E}_4)} + \frac{i^2}{(\tilde{E}_2 + \tilde{E}_3)(\tilde{E}_3 + \tilde{E}_4)} \right]. \quad (29)$$

This concludes the computation of the Fourier transform $\hat{\mathbb{1}}_{\vec{\sigma}_3}$. The edge-contraction operation can be used to compute $\hat{\mathbb{1}}_{\vec{\sigma}}$ for any orientation $\vec{\sigma}$.

4.2 Aside on parallel edges

We can also see eq. (28), in which we performed the integration of the bubble explicitly, as a result of the contraction operation with vertex choice given by v_3 : whenever two or more edges connect the same two vertices, they must be contracted all at once (see ref. [2] for details). In a formula:

$$\begin{array}{c} v_1 \\ \begin{array}{c} \leftarrow e_1 \\ \leftarrow e_2 \\ \dots \\ \leftarrow e_n \\ v_2 \end{array} \end{array} = \frac{i}{\sum_{i=1}^n \tilde{E}_i} v_{12} = \frac{i}{\sum_{i=1}^n \tilde{E}_i}. \quad (30)$$

This relation is used independently of whether it appears at the last iteration of the edge-contraction procedure or not. The general rule, for an arbitrarily complicated graph, is the following: if, at any point, the choice of vertex requires to contract parallel edges, they should be contracted all at once. Consider, for example, the following orientation of the dunce's hat

$$\begin{array}{c} v_1 \\ \begin{array}{c} \xrightarrow{e_1} v_2 \\ \leftarrow e_3 \\ \leftarrow e_2 \\ \leftarrow e_4 \\ v_3 \end{array} \end{array} = \frac{i}{\tilde{E}_1 + \tilde{E}_2 + \tilde{E}_3} \left[\begin{array}{c} v_{12} \\ \leftarrow e_3 \\ \leftarrow e_4 \\ v_3 \end{array} + \begin{array}{c} v_{13} \\ \leftarrow e_1 \\ \leftarrow e_4 \\ \leftarrow e_2 \\ v_2 \end{array} \right] \quad (31)$$

having chosen the vertex v_1 to perform edge-contraction. The second edge-contracted graph has a directed cycle. Thus, it evaluates to zero, and we can iterate the edge-contraction operation

$$\begin{array}{c} v_1 \\ \begin{array}{c} \xrightarrow{e_1} v_2 \\ \leftarrow e_3 \\ \leftarrow e_2 \\ \leftarrow e_4 \\ v_3 \end{array} \end{array} = \frac{i}{\tilde{E}_1 + \tilde{E}_2 + \tilde{E}_3} \begin{array}{c} v_{12} \\ \leftarrow e_3 \\ \leftarrow e_4 \\ v_3 \end{array} = \frac{i}{\tilde{E}_1 + \tilde{E}_2 + \tilde{E}_3} \frac{i}{\tilde{E}_3 + \tilde{E}_4}. \quad (32)$$

Having understood the treatment of parallel edges, we return to the box example.

4.3 Another example

We now look at another orientation, corresponding to $\vec{\sigma}_4 = (-1, 1, -1, -1)$. Again, we may define $\tilde{E}_i = E_i - (\vec{\sigma}_4)_i p_i^0$, and write

$$\begin{array}{c} v_1 \\ \begin{array}{c} \xrightarrow{e_2} v_2 \\ \leftarrow e_1 \\ \leftarrow e_3 \\ \leftarrow e_4 \\ v_4 \end{array} \end{array} = \int \left[\prod_{j=1}^4 d\tau_j \Theta(\tau_j) e^{i\tilde{E}_j \tau_j} \right] \delta(-\tau_1 + \tau_2 - \tau_3 - \tau_4). \quad (33)$$

Let us apply the contraction operation. We start from v_1 and obtain

$$\begin{array}{c} v_1 \xrightarrow{e_2} v_2 \\ \uparrow e_1 \quad \uparrow e_3 \\ v_4 \xrightarrow{e_4} v_3 \end{array} = \frac{i}{(\tilde{E}_1 + \tilde{E}_2)} \left[\begin{array}{c} v_{12} \\ \uparrow e_1 \quad \uparrow e_3 \\ v_4 \xrightarrow{e_4} v_3 \end{array} + \begin{array}{c} v_2 \\ \uparrow e_2 \quad \uparrow e_3 \\ v_{14} \xrightarrow{e_4} v_3 \end{array} \right]. \quad (34)$$

The first contracted graph we obtain has a directed cycle, and thus evaluates to zero. In other words, we can simply write:

$$\begin{array}{c} v_1 \xrightarrow{e_2} v_2 \\ \uparrow e_1 \quad \uparrow e_3 \\ v_4 \xrightarrow{e_4} v_3 \end{array} = \frac{i}{(\tilde{E}_1 + \tilde{E}_2)} \begin{array}{c} v_2 \\ \uparrow e_2 \quad \uparrow e_3 \\ v_{14} \xrightarrow{e_4} v_3 \end{array}. \quad (35)$$

To iterate the contraction operation, we now choose v_{14} . We obtain

$$\begin{array}{c} v_1 \xrightarrow{e_2} v_2 \\ \uparrow e_1 \quad \uparrow e_3 \\ v_4 \xrightarrow{e_4} v_3 \end{array} = \frac{i}{(\tilde{E}_1 + \tilde{E}_2)} \frac{i}{(\tilde{E}_2 + \tilde{E}_4)} \left[\begin{array}{c} v_{124} \\ \uparrow e_4 \quad \uparrow e_3 \\ v_3 \end{array} + \begin{array}{c} v_{134} \\ \uparrow e_2 \quad \uparrow e_3 \\ v_2 \end{array} \right] = \frac{i}{(\tilde{E}_1 + \tilde{E}_2)} \frac{i}{(\tilde{E}_2 + \tilde{E}_4)} \begin{array}{c} v_{134} \\ \uparrow e_2 \quad \uparrow e_3 \\ v_2 \end{array}. \quad (36)$$

To iterate one last time, we choose the vertex v_2 and contract all parallel edges (e_2 and e_3) at once, giving

$$\begin{array}{c} v_1 \xrightarrow{e_2} v_2 \\ \uparrow e_1 \quad \uparrow e_3 \\ v_4 \xrightarrow{e_4} v_3 \end{array} = \frac{i}{(\tilde{E}_1 + \tilde{E}_2)} \frac{i}{(\tilde{E}_2 + \tilde{E}_4)} \frac{i}{(\tilde{E}_2 + \tilde{E}_3)}. \quad (37)$$

This terminates the recursion.

5. Cross-Free Families

The choice of vertices that we performed at each iteration of the edge-contraction procedure is, in reality, not completely unconstrained, and engineered in order to obtain a result in a certain form. The specific set of rules that we are interested in, and that we followed in the examples above, is summarised in two constraints; at each iteration of the edge-contraction procedure, one must choose a vertex v such that:

- v is a sink or a source of the directed graph, meaning that all the arrows associated to the edges adjacent to it must either point towards v or out of v .
- the complement of v , namely the subgraph with vertices given by $\mathcal{V} \setminus \{v\}$ and edges given by $\{\{v, v'\} \in \mathcal{E} \mid v, v' \in \mathcal{V} \setminus S\}$, must be connected.

It is relatively easy to check that the choices of the previous section indeed satisfy these two rules. For example, for the diagram

$$\begin{array}{c} v_1 \xrightarrow{e_2} v_2 \\ \uparrow e_1 \quad \uparrow e_3 \\ v_4 \xrightarrow{e_4} v_3 \end{array}, \quad (38)$$

only the choices v_1 and v_2 satisfy the two constraints above. While all vertex choices satisfy the second constraint (for example, the complement of v_1 , the graph $(\{v_2, v_3, v_4\}, \{e_3, e_4\})$, is connected), v_1 and v_2 are the only sinks and sources of the graph. The existence, at each iteration of the edge-contraction procedure, of at least two vertices (at least one sink and at least one source) satisfying the properties above is guaranteed in general by the acyclic property of the graph. We will now see how this choice impacts the threshold singularity structure of the graph.

5.1 Boundary operator

For future use, let us introduce the boundary operator. For a set $S \subseteq \mathcal{V}$ of vertices, we have

$$\partial(S) = \{e = \{v, v'\} \in \mathcal{E} \mid v \in S, v' \notin S \text{ or } v' \in S, v \notin S\}. \quad (39)$$

For the labelling given in eq. (3) we have, for example, $\partial(\{v_1\}) = \{e_1, e_2\}$ (so that the boundary operator applied on a vertex simply gives the edges adjacent to that vertex) and $\partial(\{v_1, v_2\}) = \{e_1, e_3\}$ (in this case, the boundary operator gives all the edges adjacent to the vertex v_{12} obtained by contracting e_2). We also define the characteristic vector, having one component for each edge of the graph:

$$\mathbf{1}^{\partial(S)} \in \{0, 1\}^4, \quad \mathbf{1}_i^{\partial(S)} = \begin{cases} 1 & \text{if } e_i \in \partial(S) \\ 0 & \text{if } e_i \notin \partial(S) \end{cases}, \quad (40)$$

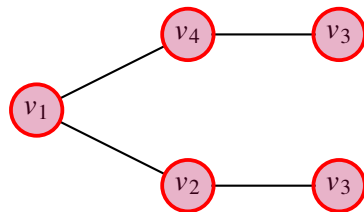
so that, for example, $\mathbf{1}^{\partial(\{v_1\})} = (1, 1, 0, 0)$. Cuts such as S can be denoted graphically by circlings: for example

$$S = \{v_1, v_4\} \Rightarrow \begin{array}{c} v_1 \quad e_2 \quad v_2 \\ \circlearrowleft \quad \square \quad \circlearrowright \\ e_1 \quad \quad e_3 \\ v_4 \quad e_4 \quad v_3 \end{array}. \quad (41)$$

The circling must contain in its interior the vertices of S , and the edges in $\partial(S)$ are those crossed by the red line of the circling, namely e_2 and e_4 .

5.2 Decision trees

Let us now interpret the result we obtained in the previous section by introducing an interesting graph-theoretic construct. Let us collect in a decision tree the choice of vertices that we made at each iteration, for the example orientation given in eq. (18). At the first iteration, we chose v_1 and got two terms; for one of them we chose v_4 , while for the other we chose v_2 ; this, after eliminating all graphs that were not acyclic, also gave us a total of two terms; at the last iteration, we choose v_3 for both of them. In other words:



The root of this tree is the starting choice of vertex, v_1 , on the utmost left. The leaves of the tree are the last choices, v_3 and v_3 , on the utmost right. We may now follow the unique path that connects each leaf to the root and collect the vertices that we encounter on the way. We find two families of subsets of vertices, corresponding to the two leaves of the tree:

$$F_1 = \{\{v_1\}, \{v_4\}, \{v_3\}\}, \quad F_2 = \{\{v_1\}, \{v_2\}, \{v_3\}\}. \quad (42)$$

For the orientation given in eq. (33), the situation is different: there is only one term at the end of the recursion, and the choices of vertices are v_1 , v_{14} and v_2 or, in tree form



The corresponding family of cuts is

$$F_3 = \{\{v_1\}, \{v_1, v_4\}, \{v_2\}\}, \quad (43)$$

where the vertex v_{14} is equivalent to the set $\{v_1, v_4\}$. These families can also be drawn using circlings: in particular, for F_3 , we draw one circling for each cut that it contains, giving



For the family F_1 , we have instead



A look at these diagrams makes it clear that the families we are investigating are constrained heavily.

5.3 Threshold singularity structure

We first observe that eq. (32) can be rewritten as

$$\begin{array}{c} v_1 \quad e_2 \quad v_2 \\ \left\{ \begin{array}{c} \leftarrow \\ \leftarrow \\ \leftarrow \end{array} \right. \\ v_4 \quad e_4 \quad v_3 \end{array} = \sum_{j=1}^2 \prod_{S \in F_j} \frac{i}{\mathbf{1}^{\partial(S)} \cdot \tilde{\mathbf{E}}^{\vec{\sigma}_3}}, \quad (46)$$

while eq. (37) can be written as

$$\begin{array}{c} v_1 \quad e_2 \quad v_2 \\ \left\{ \begin{array}{c} \leftarrow \\ \leftarrow \\ \leftarrow \end{array} \right. \\ v_4 \quad e_4 \quad v_3 \end{array} = \prod_{S \in F_3} \frac{i}{\mathbf{1}^{\partial(S)} \cdot \tilde{\mathbf{E}}^{\vec{\sigma}_4}}, \quad (47)$$

where we introduced the symbol $\tilde{\mathbf{E}}^{\vec{\sigma}}$ such that $(\tilde{\mathbf{E}}^{\vec{\sigma}})_i = E_i - \vec{\sigma}_i p_i^0$. Furthermore, the families F_1 , F_2 and F_3 satisfy striking properties:

$$+ \text{Diagram 1} + \text{Diagram 2} + \text{Diagram 3} \quad (50)$$

What is the convenience of the Cross-Free Family representation, then? The denominator, appearing in eq. (49), in the form $(\tilde{E}_1 + \tilde{E}_2 + \tilde{E}_3 + \tilde{E}_4)$, does not appear in the Cross-Free Family representation. In other words, it corresponds to a *spurious singularity* of the Time-Ordered Perturbation Theory representation. Such denominator corresponds to a cut, the middle one appearing in all the TOPT diagrams and that cuts all edges of the graph, that divides the graph in four connected components (the four singleton vertices obtained by deleting the edges crossed by the cut). This rule is indeed in contradiction with that characterising the three families F_1 , F_2 and F_3 from the previous section.

7. Conclusion

We have shown how to derive the Cross-Free Family representation for the box diagrams and used it to constrain its singularity structure. The Cross-Free Family representation has numerical advantages, in that it is a) relatively compact when compared to that of ref. [9], especially when numerators are involved, b) numerically stable, since it does not have spurious singularities. The Cross-Free Family representation also has numerous theoretical advantages: the absence of spurious singularities primes it to be a central tool in the singularity analysis of Feynman diagrams and related proofs (such as that of ref. [1]). In the future, it would be interesting to study its consequences on the analytic structure of Feynman diagrams (see, for example, the use of Time Ordered Perturbation Theory [21] to this end). The privileged role of the principle of connectedness in the Cross-Free Family representation unveils the diagrammatic manifestation of the cluster decomposition principle: for this reason, it would be interesting to study an operator-level derivation of the Cross-Free Family representation, analogous to that yielding the TOPT representation [30].

References

- [1] Zeno Capatti, Valentin Hirschi, Andrea Pelloni, and Ben Ruijl. Local Unitarity: a representation of differential cross-sections that is locally free of infrared singularities at any order. *JHEP*, 04:104, 2021.
- [2] Zeno Capatti. Exposing the threshold structure of loop integrals. *Phys. Rev. D*, 107(5):L051902, 2023.
- [3] J. Jesus Aguilera-Verdugo, Felix Driencourt-Mangin, Roger J. Hernández-Pinto, Judith Plenter, Selomit Ramirez-Uribe, Andres E. Renteria Olivo, German Rodrigo, German F. R. Sborlini, William J. Torres Bobadilla, and Szymon Tracz. Open loop amplitudes and causality to all orders and powers from the loop-tree duality. *Phys. Rev. Lett.*, 124(21):211602, 2020.
- [4] J. Jesús Aguilera-Verdugo, Roger J. Hernández-Pinto, Germán Rodrigo, German F. R. Sborlini, and William J. Torres Bobadilla. Mathematical properties of nested residues and their application to multi-loop scattering amplitudes. *JHEP*, 02:112, 2021.

- [5] Isabella Bierenbaum, Stefano Catani, Petros Draggiotis, and German Rodrigo. A tree-loop duality relation at two loops and beyond. *JHEP*, 10:073, 2010.
- [6] William J. Torres Bobadilla. Lotty – the loop-tree duality automation. *Eur. Phys. J. C*, 81(6):514, 2021.
- [7] Michael Borinsky, Zeno Capatti, Eric Laenen, and Alexandre Salas-Bernárdez. Flow-oriented perturbation theory. 10 2022.
- [8] Zeno Capatti, Valentin Hirschi, Dario Kermanschah, and Ben Ruijl. Loop-tree duality for multiloop numerical integration. *Phys. Rev. Lett.*, 123(15):151602, 2019.
- [9] Zeno Capatti, Valentin Hirschi, Dario Kermanschah, Andrea Pelloni, and Ben Ruijl. Manifestly causal loop-tree duality. 9 2020.
- [10] Stefano Catani, Tanju Gleisberg, Frank Krauss, German Rodrigo, and Jan-Christopher Winter. From loops to trees by-passing Feynman’s theorem. *JHEP*, 09:065, 2008.
- [11] Sascha Kromin, Niklas Schwanemann, and Stefan Weinzierl. Amplitudes within causal loop-tree duality. 8 2022.
- [12] Selomit Ramírez-Uribe, Roger J. Hernández-Pinto, German Rodrigo, Germán F. R. Sborlini, and William J. Torres Bobadilla. Universal opening of four-loop scattering amplitudes to trees. *JHEP*, 04:129, 2021.
- [13] Selomit Ramírez-Uribe, Roger J. Hernández-Pinto, Germán Rodrigo, and German F. R. Sborlini. From five-loop scattering amplitudes to open trees with the Loop-Tree Duality. 11 2022.
- [14] Robert Runkel, Zoltán Szőr, Juan Pablo Vesga, and Stefan Weinzierl. Causality and loop-tree duality at higher loops. *Phys. Rev. Lett.*, 122(11):111603, 2019. [Erratum: *Phys.Rev.Lett.* 123, 059902 (2019)].
- [15] Robert Runkel, Zoltán Szőr, Juan Pablo Vesga, and Stefan Weinzierl. Integrands of loop amplitudes within loop-tree duality. *Phys. Rev. D*, 101(11):116014, 2020.
- [16] German F. R. Sborlini. Geometrical approach to causality in multiloop amplitudes. *Physical Review D*, 104(3), Aug 2021.
- [17] Samuel Abreu, Ruth Britto, Claude Duhr, and Einan Gardi. From multiple unitarity cuts to the coproduct of Feynman integrals. *JHEP*, 10:125, 2014.
- [18] Samuel Abreu, Ruth Britto, Claude Duhr, and Einan Gardi. Cuts from residues: the one-loop case. *JHEP*, 06:114, 2017.
- [19] Paolo Benincasa and William J. Torres Bobadilla. Physical representations for scattering amplitudes and the wavefunction of the universe. *SciPost Phys.*, 12(6):192, 2022.
- [20] Marko Berghoff and Dirk Kreimer. Graph complexes and Feynman rules. 8 2020.

- [21] Jacob L. Bourjaily, Holmfridur Hannesdottir, Andrew J. McLeod, Matthew D. Schwartz, and Cristian Vergu. Sequential Discontinuities of Feynman Integrals and the Monodromy Group. *JHEP*, 01:205, 2021.
- [22] Einan Gardi, Franz Herzog, Stephen Jones, Yao Ma, and Johannes Schlenk. The on-shell expansion: from Landau equations to the Newton polytope. 11 2022.
- [23] Holmfridur S. Hannesdottir and Sebastian Mizera. What is the $i\epsilon$ for the S-matrix? 4 2022.
- [24] Dirk Kreimer. *Outer Space as a Combinatorial Backbone for Cutkosky Rules and Coactions*. 2021.
- [25] Dirk Kreimer and Karen Yeats. Algebraic interplay between renormalization and monodromy. 5 2021.
- [26] Sinai Robins. A friendly introduction to Fourier analysis on polytopes.
- [27] George Sterman and Aniruddha Venkata. Local infrared safety in time-ordered perturbation theory. 9 2023.
- [28] George F. Sterman. Partons, factorization and resummation, TASI 95. In *Theoretical Advanced Study Institute in Elementary Particle Physics (TASI 95): QCD and Beyond*, pages 327–408, 6 1995.
- [29] George F. Sterman. *An Introduction to quantum field theory*. Cambridge University Press, 8 1993.
- [30] M.D. Schwartz. *Quantum Field Theory and the Standard Model*. Quantum Field Theory and the Standard Model. Cambridge University Press, 2014.